Acoustic frequency-based differentiation of photoacoustic signals from surgical biomarkers

Eduardo A. Gonzalez*and Muyinatu A. Lediju Bell*†‡
*Department of Biomedical Engineering, Johns Hopkins University, Baltimore, MD
†Department of Electrical and Computer Engineering, Johns Hopkins University, Baltimore, MD
‡Department of Computer Science, Johns Hopkins University, Baltimore, MD

***Abstract*—Spectral unmixing techniques for photoacoustic images are often used to isolate signal origins (e.g., blood, contrast agents, lipids). However, these techniques tend to exploit the optical properties of different biological chromophores and do not typically consider acoustic properties. Analysis of the acoustic frequency response of photoacoustic signals has the potential to provide additional discrimination of photoacoustic responses from different materials, with the added benefit of potentially requiring few optical wavelength emissions. This study presents our initial results testing this hypothesis in a phantom experiment, given the task of differentiating between photoacoustic signals from deoxygenated hemoglobin (Hb) and methylene blue (MB). Coherence-based beamforming, principal component analysis, and nearest neighbor classification were employed to determine ground-truth labels, perform feature extraction, and classify image contents, respectively. The mean $\pm$ one standard deviation of classification accuracy was increased from 0.67 $\pm$ 0.05 to 0.81 $\pm$ 0.11 when increasing the number of wavelength emissions from one to two, respectively. When using an optimal laser wavelength pair of 690 and 870 nm, the sensitivity and specificity of detecting MB over Hb were 1.00 and 1.00, respectively. Results are highly promising for the differentiation of photoacoustic-sensitive materials with comparable performance to that achieved with a more conventional multispectral laser wavelength approach.**

***Index Terms*—photoacoustic imaging, spectral unmixing, nearest neighbour classification, frequency analysis, principal component analysis.**

I. Introduction

In photoacoustic imaging, spectral unmixing techniques [1] are often used to isolate signal origins (e.g., blood, contrast agents, lipids) with one goal of discriminating among biomarkers during surgical interventions. These techniques consist of generating an overdetermined system of equations (i.e., more equations than variables) from the signal response of each chromophore at different laser wavelengths, which can then be solved with an optimization technique based on the known optical absorption coefficient for each chromophore at each wavelength. For example, Xia *et al.* [2] used a pseudo inverse approach to differentiate photoacoustic responses originating from water, blood, and lipids, as well as differentiating photoacoustic responses originating from tendons and nerves [3]. More recently, Grasso *et al.* [4] proposed an iterative approach to discriminate blood oxygenation levels by solving the system of equations with a non-negative matrix factorization, compensating for the ill-conditioned invertibility of the absorption coefficient matrix. Despite their effectiveness, these spectral unmixing techniques are typically infeasible for most real-time applications because of the long overall acquisition times associated with transmitting multiple laser wavelengths. Traditional spectral unmixing techniques also do not typically consider differences in acoustic spectra, which has the potential to provide additional information for differentiation between biomarkers or different soft tissues, similar to the information provided by spectral parameter classifications [5].

As an example of spectral parameters classification, Cao *et al.* [6] used the acoustic spectra filtered with the frequency response of the ultrasound transducer to conduct a k-means clustering between photoacoustic signals originating from olive oil and cholesterol. However, this spectral parameter classification approach has three limitations. First, in contrast to spectral unmixing techniques, labelled regions are required. Second, these labelled regions rely on *a priori* information about the location of materials to be differentiated. Third, spectral parameters provide a limited snapshot of frequency characteristics. These three limitations diminish feasibility for image guidance during surgical interventions and reduce classification performance.

To overcome the challenges described above with regard to traditional spectral unmixing [2], [4] and spectral parameter classification [6], we propose a novel, more general acoustic frequency-based analysis method to discriminate photoacoustic responses from different materials. This method operates directly on the magnitude of the pressure signals to provide richer analysis information, presenting two key benefits. First, the method uses the full baseband spectra (i.e., it does not filter the spectra to the frequency response of the transducer). Second, the method applies a classification framework using a training and testing set of known photoacoustic-sensitive materials (i.e., no *a priori* signal location information is required). We hypothesize that this method, which relies on an analysis of the acoustic frequency response from a single or dual wavelength emission, is sufficient to differentiate biomarkers and has the potential to increase possible frame rates for real-time implementation in the operating room.

This paper presents initial results testing our hypothesis. A frequency analysis was applied to the received photoacoustic signals from two materials (i.e., blood and methylene blue) injected in a plastisol phantom. The baseband frequency spectra were then transformed to a reduced feature space through principal component analysis (PCA) and the two signal contents were identified using nearest neighbor clas-

978-1-7281-5448-0/20/$31.00 ©2020 IEEE

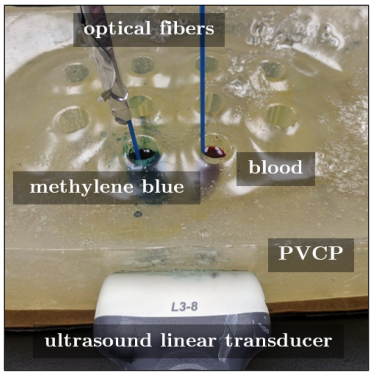

Fig. 1. Acquisition setup to test the differentiation of methylene blue (MB) from blood (Hb). These photoacoustic-sensitive materials fill the hollow chambers of a custom polyvinyl chloride plastisol (PVCP) phantom.

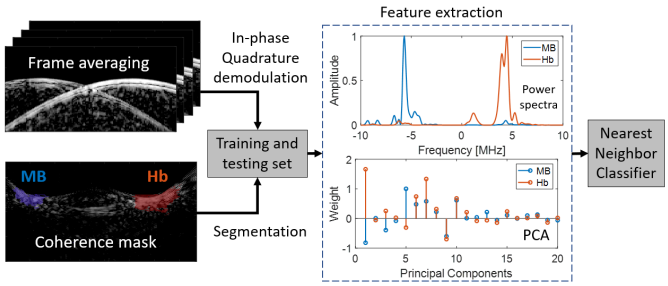

Fig. 2. Overview of proposed method to differentiate photoacoustic signal sources using acoustic frequency information. The blue and red coherence masks show regions of interest for methylene blue (MB) and blood (Hb), respectively. Spectra are asymmetric with respect to frequency because baseband signals were analyzed after IQ demodulation.

sification. The necessity to differentiate blood and methylene blue is motivated by recently proposed photoacoustic-guided hysterectomy techniques that require differentiation of uterine arteries from ureters containing methylene blue [7].

II. Method

Fig. 1 shows the experimental setup used to differentiate two photoacoustic-sensitive materials. A polyvinyl chloride-plastisol (PVCP) was fabricated with length, width, and height of 29 cm, 18 cm, and 10 cm, respectively. The phantom was modified with ten cylindrical hollow chambers. Each of these chambers had a diameter of 15 mm and a depth of 55 mm. Two of the hollow chambers were filled with a 1% weight-by-volume aqueous solution of methylene blue (MB) and human blood (Hb), and a 1-mm-diameter optical fiber was inserted in each of the filled chambers. These fibers originated from a bifurcated fiber bundle that was connected to a Phocus Mobile laser (Opotek Inc., Carlsbad, CA, USA), transmitting laser light with wavelengths ranging from 690-950 nm in 10 nm increments. The tip of each optical fiber was positioned approximately 15 mm below the top surface of the chambers, and photoacoustic signals were generated with an energy of 4 mJ at each fiber tip. By transmitting light individually into each chamber, the differences in amplitude response caused by fluence differences were minimized. The generated photoacoustic signals were received by an Alpinion L3-8 linear array ultrasound probe that was positioned on the lateral wall of the phantom, approximately 40 mm away from the hollow chamber cross section, as shown in Fig. 1.

Fig. 2 shows a summary of the framework for differentiating photoacoustic signals sources. Raw data from each wavelength were first averaged over 10 acquisitions to reduce incoherent noise. Photoacoustic images were then generated using conventional delay-and-sum (DAS) beamforming. Two regions of interest (ROI) were defined to separate photoacoustic signals generated from MB and Hb, located on the right and the left sides of the photoacoustic images, respectively. Ground-truth labels were segmented from locally weighted short-lag spatial coherence (LW-SLSC) images [8] (i.e., a newer variant of short-lag spatial coherence (SLSC) [9] beamforming), using a regularization factor of $\alpha = 1$ and an axial correlation kernel of 2λ, where λ is the wavelength associated with the center frequency of the L3-8 ultrasound probe. Binary segmentation was performed using a -6 dB threshold mask applied to the LW-SLSC images.

A frequency analysis was performed over the magnitude of the pressure waves, which were either zero or positive, rather than the original pressure waves used for conventional beamforming, which have negative and positive values. For each material (i.e., MB and Hb), the normalized power spectra were calculated from a sliding window of axial kernels of in-phase and quadrature (IQ) data (which was converted to baseband with a modulation frequency of 2.5 MHz and a bandpass filter of 200% bandwidth), each 3.85 mm in length. Principal component analysis (PCA) was applied to the power spectra of photoacoustic signals acquired at each laser wavelength in order to reduce the length of each power spectra to its first 20 principal components. Finally, nearest neighborhood (NN) classification was applied with the L2-norm as the measure of distance. MB and Hb were considered as positive and negative samples, respectively, for the estimation of accuracy, sensitivity, and specificity metrics.

Fig. 3 shows two proposed spectral analyses: (1) dual wavelength and (2) single wavelength. In the dual wavelength analysis, the IQ spectra of the photoacoustic response from a region of interest using two different wavelengths were stacked

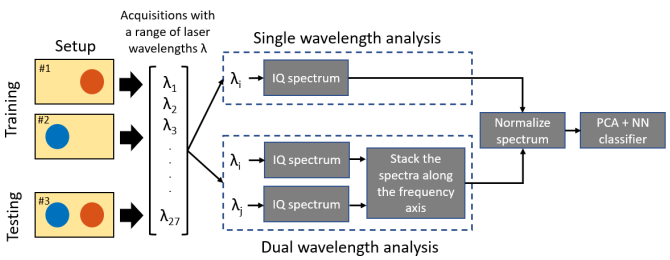

Fig. 3. Two proposed spectral analyses for characterizations based on single (top) and dual (bottom) wavelength emissions.

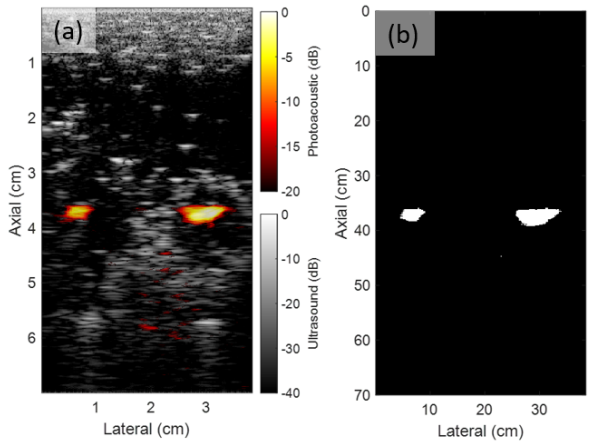

Fig. 4. (a) Locally-weighted short-lag spatial coherence (LW-SLSC) photoacoustic image overlaid on a DAS ultrasound image of MB (left) and Hb (right), obtained with a laser wavelength emission of 950 nm. (b) Segmented masks for MB and Hb after a -6 dB threshold was applied to the LW-SLSC photoacoustic image.

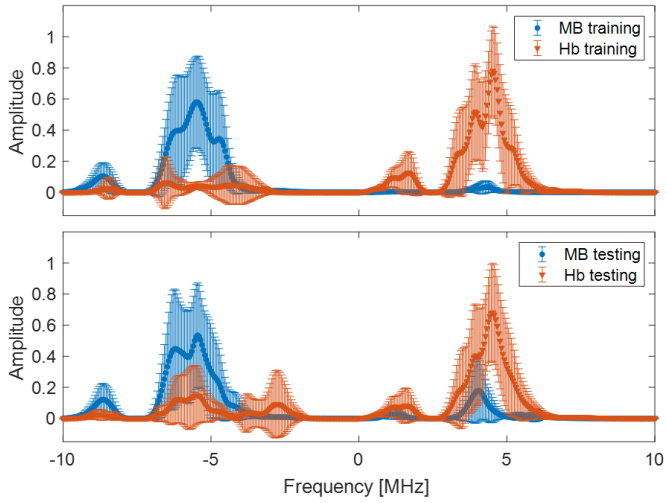

Fig. 5. Examples of (top) training and (bottom) testing spectra of in-phase quadrature data from MB and Hb. The spectra show combined results obtained with 690 nm and 870 nm laser wavelength (dual wavelength analysis).

and normalized to enhance differences in frequency content. No stacking was required for the single wavelength analysis.

III. Results and Discussion

Fig. 4(a) shows an example LW-SLSC photoacoustic image co-registered to a DAS ultrasound image obtained with a laser wavelength of 950 nm. Fig. 4(b) shows the corresponding segmentation mask. The coherence-based LW-SLSC imaging approach enabled successful segmentation and isolation of the signals of interest.

Fig. 5 shows examples of stacked spectra (dual wavelength analysis) of MB and Hb for 690 nm and 870 nm laser wavelengths. The mean and standard deviation of the spectra were generated by averaging all kernels of MB and Hb for the training and testing set. In contrast to the single wavelength analysis, the normalized spectra from stacking two wavelength responses enhance the differentiation of MB and Hb.

Fig. 6 shows the NN classification sensitivity and specificity when using single wavelengths in the range of 690 nm to 950 nm. The mean $\pm$ one standard deviation of sensitivity and specificity was 0.69 ± 0.22 and 0.53 ± 0.15, respectively, and the overall accuracy was 0.67 ± 0.05. The optimal wavelength that yielded the highest sensitivity and specificity was 880 nm (0.83 sensitivity and 0.69 specificity). Overall, these results show a low classification performance when attempting to discriminate photoacoustic signal by using the shape (and not the amplitude) of the normalized spectrum of a single wavelength.

Fig. 7 shows the NN classification sensitivity and specificity when using a pair of wavelengths in the range of 690 nm to 950 nm. The mean $\pm$ one standard deviation of sensitivity and specificity was 0.89 ± 0.20 and 0.74 ± 0.16, respectively, and the overall accuracy was 0.82 ± 0.11. The optimal wavelength pair that yielded the highest sensitivity and specificity was 690 nm and 870 nm with a sensitivity of 1.000 and a specificity of 1.00.

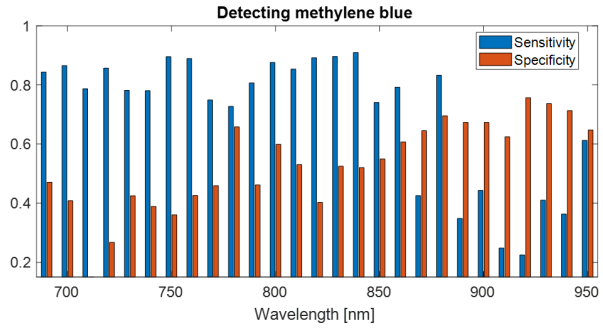

Fig. 6. Mean sensitivity and specificity when using the single wavelength analysis setup. When considering wavelengths from 690 nm to 950 nm, the mean $\pm$ one standard deviation of sensitivity and specificity was 0.69 ± 0.22 and 0.53 ± 0.15, respectively. The laser wavelength that reported the highest combined sensitivity and specificity was 880 nm with a sensitivity of 0.83 and specificity of 0.69.

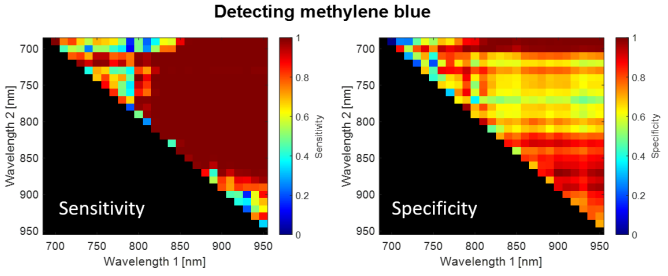

Fig. 7. Mean sensitivity and specificity when using the dual wavelength analysis setup. When considering wavelengths from 690 nm to 950nm, the mean $\pm$ one standard deviation of sensitivity and specificity was 0.89 ± 0.20 and 0.74 ± 0.16, respectively. The pair of laser wavelength that reported the highest combined sensitivity and specificity was 690 nm and 870 nm with a sensitivity of 1.00 and specificity of 1.00. The black region indicates redundant entries that were not tested twice (only unique wavelength pairs were tested).

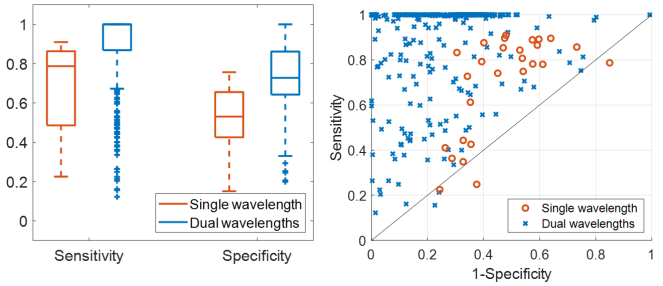

Fig. 8. Comparison of sensitivity and specificity from single and dual wavelengths analyses with (left) box plots and (right) sensitivity vs. 1-specificity for the performance of each individual classifier.

Fig. 8 shows a comparative summary of the sensitivity and specificity results when using the single and dual wavelength analyses with our proposed method. Specifically, Fig. 8(a) shows the box plots of sensitivity and specificity for both analyses, where the horizontal lines represent the median, the upper and lower edges of each box represent the upper and lower quartiles of each data set, the top and bottom lines extending from the boxes indicate the maximum and minimum of each data set, and the crosses indicate outliers defined as any value larger than 1.5 times the interquartile range. Fig. 8(b) shows the same results as individual classifier performance in an ROC-curve format. By assuming a threshold of 0.90 specificity and 0.90 specificity as good classification performance, 38 wavelengths pairs were found in the dual wavelength analysis while no cases were found for the single wavelength analysis.

Overall, the performance achieved with the dual wavelength analysis was comparable to spectral unmixing method requiring 29 [2] to 45 [4] wavelengths, and to an acoustic frequency-based segmentation method [6]. When implementing the spectral unmixing methods described by Xia *et al.* [2] to differentiate between Hb and MB with 12 wavelengths emissions (i.e., from 690 nm to 800 nm in 10 nm increments) of 10 frames each, the mean sensitivity and specificity was 0.84 and 0.99, respectively. Similarly, the non-negative matrix factorization method described by Grasso *et al.* [4] achieved a mean sensitivity and specificity of 0.86 and 0.99, respectively. Finally, the acoustic-based clustering method from Cao *et al.* [6] achieved a mean sensitivity and specificity of 0.84 and 0.78, respectively, when averaging over the 27 wavelength emissions. The best performance using the method in [6] with a single wavelength emission occurred for a laser wavelength of 940 nm, resulting in a mean sensitivity and specificity of 1.00 and 0.96, respectively.

IV. Conclusions

We developed a novel frequency-based photoacoustic classifier to distinguish photoacoustic-sensitive materials. This classifier employs coherence-based beamforming, principal component analysis, and nearest neighbor classification in order to build an atlas of photoacoustic spectra specific to methylene blue and blood. Results are highly promising for the differentiation of photoacoustic-sensitive materials using radiofrequency information from only two wavelength emissions, with comparable performance to that achieved with a more conventional multispectral approach.

Acknowledgments

This work was supported by NSF CAREER Award ECCS-1751522. The authors acknowledge the support of NVIDIA Corporation with the donation of the Titan Xp GPU used for this research.

References

[1] J. Glatz, N. C. Deliolanis, A. Buehler, D. Razansky, and V. Ntziachristos, "Blind source unmixing in multi-spectral optoacoustic tomography," *Optics Express*, vol. 19, no. 4, pp. 3175–3184, 2011.

[2] W. Xia, S. J. West, D. I. Nikitichev, S. Ourselin, P. C. Beard, and A. E. Desjardins, "Interventional multispectral photoacoustic imaging with a clinical linear array ultrasound probe for guiding nerve blocks," in *Photons Plus Ultrasound: Imaging and Sensing 2016*, vol. 9708. International Society for Optics and Photonics, 2016, p. 97080C.

[3] J. M. Mari, W. Xia, S. J. West, and A. E. Desjardins, "Interventional multispectral photoacoustic imaging with a clinical ultrasound probe for discriminating nerves and tendons: an ex vivo pilot study," *Journal of biomedical optics*, vol. 20, no. 11, p. 110503, 2015.

[4] V. Grasso, J. Holthof, and J. Jose, "An automatic unmixing approach to detect tissue chromophores from multispectral photoacoustic imaging," *Sensors*, vol. 20, no. 11, p. 3235, 2020.

[5] R. E. Kumon, C. X. Deng, and X. Wang, "Frequency-domain analysis of photoacoustic imaging data from prostate adenocarcinoma tumors in a murine model," *Ultrasound in Medicine & Biology*, vol. 37, no. 5, pp. 834–839, 2011.

[6] Y. Cao, A. Kole, L. Lan, P. Wang, J. Hui, M. Sturek, and J.-X. Cheng, "Spectral analysis assisted photoacoustic imaging for lipid composition differentiation," *Photoacoustics*, vol. 7, pp. 12–19, 2017.

[7] A. Wiacek, K. C. Wang, H. Wu, and M. A. L. Bell, "Dual-wavelength photoacoustic imaging for guidance of hysterectomy procedures," in *Advanced Biomedical and Clinical Diagnostic and Surgical Guidance Systems XVIII*, vol. 11229. International Society for Optics and Photonics, 2020, p. 112291D.

[8] E. Gonzalez and M. A. L. Bell, "Segmenting bone structures in ultrasound images with locally weighted slsc (lw-slsc) beamforming," in *2018 IEEE International Ultrasonics Symposium (IUS)*. IEEE, 2018, pp. 1–9.

[9] M. A. Lediju, G. E. Trahey, B. C. Byram, and J. J. Dahl, "Short-lag spatial coherence of backscattered echoes: Imaging characteristics," *IEEE Transactions on Ultrasonics, Ferroelectrics, and Frequency Control*, vol. 58, no. 7, pp. 1377–1388, 2011.